Hysteresis and creep modeling and compensation for a piezoelectric actuator using a fractional-order Maxwell resistive capacitor approach

Hysteresis and creep modeling and compensation for a piezoelectric actuator using a fractional-order Maxwell resistive capacitor approach

Yanfang Liu[1,2], Jinjun Shan[2], Ulrich Gabbert[3] and Naiming Qi[1]

[1] Department of Aerospace Engineering, Harbin Institute of Technology, Harbin,
People's Republic of China
[2] Department of Earth and Space Science and Engineering, York University, Toronto, Canada
[3] Institut für Mechanik (IFME), Otto-von-Guericke-Universität Magdeburg, Magdeburg, Germany

E-mail: yfliu@sdcnlab.esse.yorku.ca, jjshan@yorku.ca, ulrich.gabbert@ovgu.de
and qinm@hit.edu.cn

Abstract
A physics-based fractional-order Maxwell resistive capacitor (FOMRC) model is proposed to
characterize nonlinear hysteresis and creep behaviors of a piezoelectric actuator (PEA). The
Maxwell resistive capacitor (MRC) model is interpreted physically in the electric domain for
PEAs. Based on this interpretation, the MRC model is modified to directly describe the
relationship between the input voltage and the output displacement of a PEA. Then a
procedure is developed to identify the parameters of the MRC model. This procedure is
capable of being carried out using the measured input and output of a PEA only. A
fractional-order dynamics is integrated into the MRC model to describe the effect of creep, as
well as the detachment of hysteresis loops caused by creep. Moreover, the inverse FOMRC
model is constructed to compensate for hysteresis and creep in an open-loop positioning
application of PEAs. Simulation and experiments are carried out to validate the proposed
model. The PEA compensated by the inverse FOMRC model shows an excellent linear
behavior.

(Some figures may appear in colour only in the online journal)

1. Introduction

Positioning stages based on piezoelectric actuators (PEAs)
are widely used in high-precision positioning and tracking
applications, e.g., atomic force microscopy, scanning tun-
neling microscopy, and diamond turning machines. These
actuators have high stiffness, fast frequency response, and
high resolution. A PEA can be driven by either voltage
or current. When driven by voltage, it comes with the
disadvantage of having to cope up with nonlinearities, mainly
hysteresis and creep.

For PEAs, hysteresis is a nonlinearity that the output
displacement depends on a combination of the currently
applied voltage as well as on some past values of the applied
voltage. Herein, hysteresis represents the rate-independent
memory effect. However, the observed hysteresis in PEAs
shows a rate-dependent phenomenon as it is always coupled
with the creep effect at low frequencies and the dynamic effect
at high frequencies. Hysteresis can lead to large positioning
errors in piezo positioners which are operated over relatively
long displacement ranges. Hysteresis is more pronounced
over longer operating ranges and can be minimized by
operating a PEA in a linear range by keeping the amplitude
of the applied voltage signal as small as possible. Lowering
the frequency of the reference signal can reduce the coupling

effects from the rate-dependent dynamics. Creep can be seen as a slow drift in the PEA displacement after responding to a sudden change in the input voltage. Creep affects absolute positioning of a PEA and is more prominent in slow and static applications. The rate and amount of creep strongly depend on the piezoelectric material. A large voltage step will produce a rapid displacement followed by a slow creeping motion, which can last several minutes. For some input voltage profiles, one can also observe simultaneous influence of hysteresis and creep on displacement responses. Operating a PEA fast enough and over a shorter duration of time can help reduce the drifting caused by the creep effect. Hysteresis and creep, together, can lead to inaccuracy in the open-loop control and instability in the closed-loop control [1].

Recently, the Spacecraft Dynamics Control and Navigation Laboratory (SDCNLab) at York University has worked with a Canadian company to develop a 2D imaging spectrometer, which provides 2D multispectral mappings for atmospheric science, meteorology and planetary mineralogy. This spectrometer employs multiple piezoelectric actuators to provide spectral tuning of the desired optical signal transmittance by selecting the gap spacing of a tunable optical filter. For this application, the requirements on the positioning of PEAs are extremely high, i.e. in the nanometer level.

One effective way to cancel hysteresis and/or creep is to construct a model that is capable of describing the nonlinearity in a PEA and then preshape the input voltage based on the model. In the open literature, Preisach [2–4] and Prandtl–Ishlinskii [5–11] operators are widely used to model the hysteresis in PEAs. Both operators belong to the class of operators with a Preisach memory and are essentially a mathematical description of observed hysteresis in smart materials. The effects of dynamic loading have to be considered separately. Goldfarb and Celanovic proposed an electromechanical model for PEAs by introducing the Maxwell-slip friction model into electric domain, which is referred to as the Maxwell resistive capacitor (MRC) model [12, 13]. This electromechanical model is completely based on physical principles and consists of an electric and a mechanical domain, as well as the energy transfer between two domains. These hysteresis models are quasi-static and well suited for rate-independent hysteresis. The observed hysteresis in PEAs shows a rate-dependent feature that is due to dynamic behavior and/or creep. The creep effect also influences PEA positioning accuracy. To cope with creep, the linear time-invariant creep model [5, 9] and logarithmic creep model [4, 6–8, 10, 11] are introduced into the hysteresis model. Both models are a phenomenological approach and give little insight into the physical principles. In [14], the authors proposed a fractional-order creep model, based on observed fractional-order dynamics in dielectric materials [15].

In this paper, a *fractional-order Maxwell resistive capacitor* (FOMRC) model is proposed by integrating the fractional-order creep into the MRC model to characterize the coupling effects of hysteresis and creep, such as the rate-dependent phenomenon and detachment of hysteresis loops. Firstly, a detailed physical interpretation of the MRC
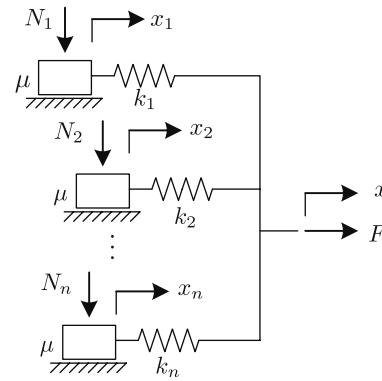

Figure 1. Maxwell-slip fiction model.

model is given for PEAs. Based on this interpretation, the MRC model is modified to map a PEA's voltage–displacement property directly. Then the fractional-order creep is integrated into the modified MRC model to further improve the model performance in slow and static applications. An identification procedure of the MRC model parameters, which is capable to be carried out only using measured input and output of a PEA, is developed. The FOMRC model is used to compensate for the nonlinearities in a PEA inversely and its validation is demonstrated by hardware experiments.

This paper is organized as follows. In section 2, the FOMRC model is proposed. A parameter identification procedure is developed in section 3. Experimental tests on the FOMRC model and the inverse compensation are shown in section 4. Section 5 concludes this paper.

2. Physical model

In this section, a physical model for a PEA is formulated. The Maxwell model in the mechanical domain, referred to as the Maxwell-slip friction model, is reviewed and its interpretation in the electric domain, referred to as the Maxwell resistive capacitor (MRC) model, is given. Then, the fractional-order creep is integrated into the MRC model to characterize the creep phenomenon. Hereafter, the new model is referred to as the *fractional-order Maxwell resistive capacitance* (FOMRC) model.

2.1. Maxwell-slip friction model in the mechanical domain

The Maxwell-slip friction model, which was also called the parallel–series Iwan model [16], is widely used to describe the pre-sliding friction [17–20]. It was initially formulated by the mathematician and physicist James C Maxwell in the mid-1800s [12]. This model is formed by putting n spring-slider elements in parallel, each of which consists of a linear spring with stiffness k_i in series with a Coulomb friction block having a breakaway force f_i (see figure 1). The constitutive behavior of the Maxwell-slip friction model can be described by

$$\dot{x}_i(t) = \begin{cases} 0 & k_i[x(t) - x_i(t)]\,\mathrm{sgn}\,\dot{x}(t) < f_i \\ \dot{x}(t) & k_i[x(t) - x_i(t)]\,\mathrm{sgn}\,\dot{x}(t) \geq f_i \end{cases} \quad (1)$$

$$F(t) = \sum_{i=1}^{n} k_i[x(t) - x_i(t)] \tag{2}$$

where x is the input displacement, F is the output force, and k_i, x_i, and $f_i = \mu_i N_i$ are the spring stiffness, block position, and breakaway force of the ith spring-slider element, respectively.

The idea of this model is as follows. When the displacement increases or decreases continuously, the gain between the force and the displacement changes piecewise linearly, which is used to fit the nonlinear gain between the input and output in the hysteresis loop. The sliding elements come to stick when the movement changes direction, which is used to characterize the sudden switch of the gain at the endpoint of the hysteresis loop. More details can be found in [17–23].

2.2. MRC model in the electric domain

Goldfarb and Celanovic [12, 13] proposed an electromechanical model for PEAs by introducing the Maxwell model into the electric domain. Their model consists of an electric and a mechanical domain, as well as the energy transfer between the two domains, see figure 2. The equation describing the mechanical part is

$$m\ddot{x}(t) + c\dot{x}(t) + kx(t) = F_T + F_{\text{ext}} \tag{3}$$

where x is the displacement, m, c, and k are the effective mass, damping, and stiffness of a PEA, and F_T and F_{ext} are forces transduced from the electric domain and imposed from the external mechanical load. The electromechanical transformer is governed by

$$F_T = T_F u_T \tag{4}$$

$$q_T = T_q x \tag{5}$$

where u_T is the voltage applied to the transformer and q_T is the charge on it, and T_F and T_q are electromechanical transformation ratios from voltage to force and from displacement to charge. In [12, 13, 21–23], these two transfer ratios were not distinguished from each other. However, as they actually have different physical interpretations, it is better to represent them by two different variables [24], even when they have the same value (which may rarely happen). The total applied voltage and charge are calculated as

$$u = u_{\text{mrc}} + u_T \tag{6}$$

$$q = Cu_T + q_T \tag{7}$$

where C is the PEA's capacity and u_{mrc} is the voltage across the MRC block. Hysteresis herein lies solely in the electric domain between u_{mrc} and q, which is described by the MRC model

$$\dot{q}_i(t) = \begin{cases} \dot{q}(t) & u_i(t)\operatorname{sgn}\dot{q}(t) < u_{S,i} \\ 0 & u_i(t)\operatorname{sgn}\dot{q}(t) \geq u_{S,i} \end{cases} \tag{8}$$

$$q_i(t) = C_i u_i(t) \tag{9}$$

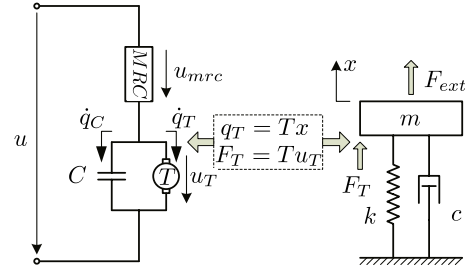$$u_{\text{mrc}}(t) = \sum_{i=1}^{n} u_i(t). \tag{10}$$

Figure 2. Electromechanical PEA model.

This electromechanical model is completely based on physical principles. Goldfarb and Celanovic gave a general interpretation arising from molecular dipoles in [13], but not in detail. The detailed interpretation here is as follows.

Even after poling, the orientations of the molecular (cell) dipoles that constitute the ceramic are not aligned perfectly [25], see figure 3(a). When an electric field is applied to a group of unit cells with the same orientation (Weiss domains), it results in two effects: surface generation of electric charge, which causes internal generation of a mechanical strain, and alignment of the domain orientation with the field, see figure 3(b). The change of domain orientation is limited under a given condition (temperature and maximum applied voltage). After the domain orientation is fully aligned with the field (or achieves the limitation), increasing the strength of the electric field causes surface generation of electric charge only, see figure 3(c). If the electric field switches its change direction, the domain experiences similar effects: both changes of surface electric charge, see figure 3(d), and domain orientation in the beginning and change of surface electric charge after the domain orientation achieving its limitation, see figure 3(e). Both stages are described by the voltage–charge graphic in figure 4(a). For simplification, the relationship between the applied voltage and the surface charge is assumed to be linear. The property given in figure 4(a) can be represented by series connection of two ideal elements: ideal capacitor and voltage-limited capacitor (see figure 4(d)). Their charge–voltage properties are shown in figures 4(b) and (c), respectively. In figure 4(d), C_e is the effective capacitance, C_s and u_S represent the capacitance and saturated voltage of the voltage-limited capacitor. Before and after the voltage-limited capacitor is saturated, the capacitances of the net are respectively $\frac{C_e C_s}{C_e + C_s}$ and C_e.

As a PEA consists of many Weiss domains, a PEA can be equivalent to the circuit in figure 5. Then the physical interpretation of the parameters in equations (8)–(10) can be given as follows: q and u are the charge and voltage applied to the PEA, q_i and u_i are the ith Weiss domain surface charge and the voltage across it, $u_{S,i}$ and $C_i = C_{s,i}$ are the saturated voltage and capacity of ith voltage-limited capacitor. The right-hand capacitor is the result of series connection of all the ideal capacitors, i.e. $1/C_{s,n+1} = \sum_{i=1}^{n} 1/C_{e,i}$, which can be treated as another voltage-limited capacitor with infinite saturated voltage, i.e. $u_{S,n+1} = \infty$.
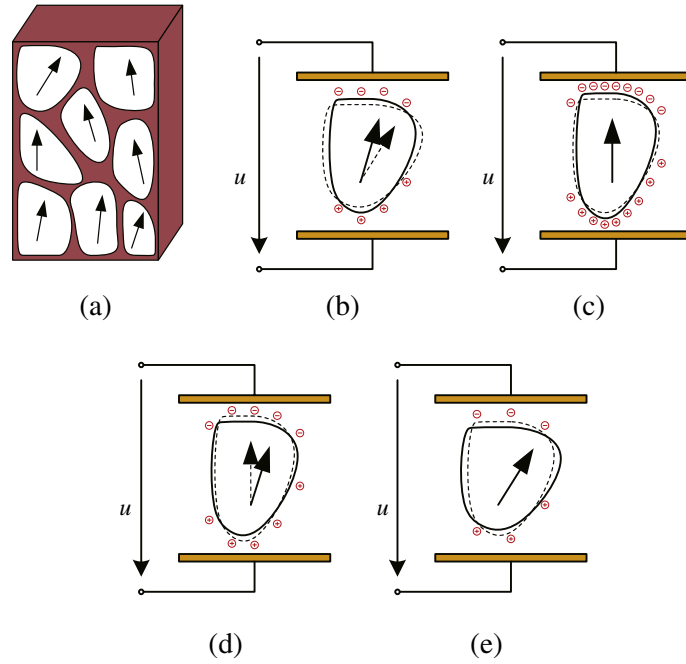
Figure 3. Behaviors of the PEA and Weiss domain when an electric field is applied: (a) molecular orientations after poling, (b) before and (c) after reaching the Weiss domain orientation limitation when the applied electric field increases or decrease continuously, (d) before and (e) after reaching the Weiss domain orientation limitation when the applied electric field switches direction of change.
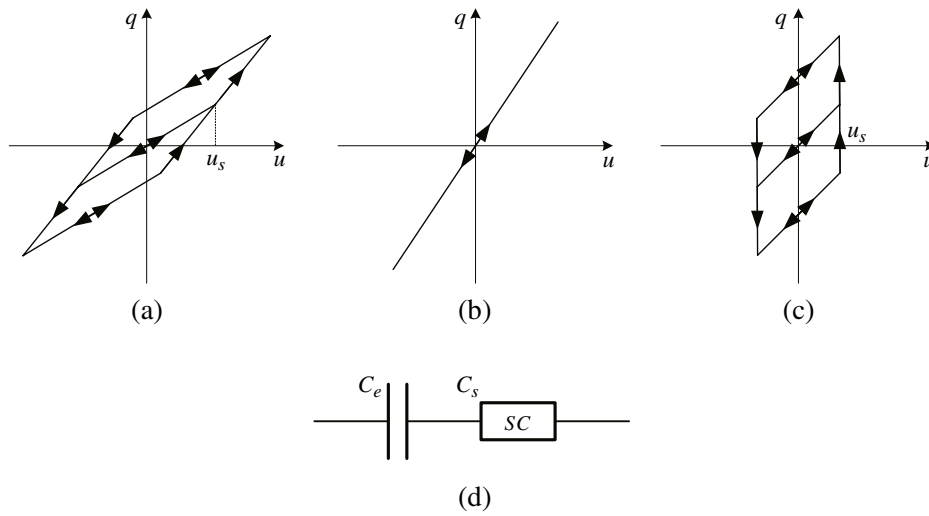

Figure 4. Voltage–charge property and equivalent circuit of the Weiss domain: (a) Weiss domain, (b) ideal capacitor, and (c) voltage-limited capacitor voltage–charge properties, (d) equivalent circuit of Weiss domain.
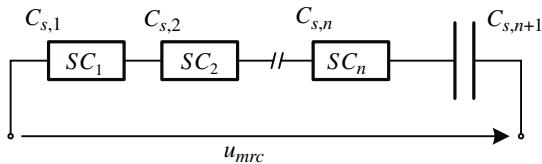

Figure 5. Equivalent circuit of PEA.

It is assumed that the excitation signal changes slowly and, then, the derivative parts in equation (3) can be neglected. With the absence of external force, equation (3) becomes

$$kx = F_{\mathrm{T}}. \tag{11}$$

By using equations (4)–(7), one obtains

$$q = (C + T_q T_F/k)u_{\mathrm{T}} = (Ck/T_F + T_q)x = T_{\mathrm{e}}x \tag{12}$$

where $T_q T_F/k$ is the electrical equivalent of the mechanical stiffness k and $T_{\mathrm{e}} = Ck/T_F + T_q$ is the effective displacement to charge electromechanical transfer ratio. This equation represents the PEA's capacitive effect. Compared with figure 5,

$$C_{\mathrm{s},n+1} = C + T_q T_F/k. \tag{13}$$

By treating the effect as an additive voltage-limited capacitor with infinite saturated voltage, as stated above,

equation (10) becomes

$$u(t) = \sum_{i=1}^{n+1} u_i(t). \quad (14)$$

Equations (12)–(14) are quite useful as the input is voltage applied to a PEA and the output is the output displacement. Thus, the data collected from a PEA positioning system can be used directly. Therefore, the modified MRC model under slow signal assumption is summarized as

$$\frac{\dot{q}_i(t)}{T_e} = \begin{cases} \dot{x}(t) & u_i(t)\,\mathrm{sgn}\,\dot{q}(t) < u_{S,i} \\ 0 & u_i(t)\,\mathrm{sgn}\,\dot{q}(t) \geq u_{S,i} \end{cases} \quad (15)$$

$$\frac{q_i(t)}{T_e} = \kappa_i u_i(t) \quad (16)$$

$$u(t) = \sum_{i=1}^{n+1} u_i(t) \quad (17)$$

where $\kappa_i = \frac{C_i}{T_e}$. In this model, the actual transfer ratios need not be known and the parameters, κ_i and $u_{S,i}$, which characterize this model, can be identified from a single set of input and output signals.

2.3. FOMRC model for creep and hysteresis

2.3.1. Creep behavior. When step voltage inputs are applied to a PEA, the corresponding responses are not proportional to the applied voltage and very slow drifts are observed from the output displacement. Figure 6(a) shows the test results, where the responses have been normalized by dividing by the input values. By assuming that all the dynamic responses except for the creep come to steady at 0.5 s, the gains are calculated by the output displacements divided by the corresponding input voltages. If the output is further normalized by the nonlinear gains, the responses are very similar, as shown in figure 6(b). This suggests that the creep and nonlinear gains can be modeled separately. Physically, the nonlinear gain is caused by hysteresis and modeled by the MRC model. In this section, the fractional-order integrator is introduced into the MRC model to characterize creep, as well as rate-dependent hysteresis and detachment of hysteresis loops.

2.3.2. Fractional-order creep model. Physically, creep is caused by a gradual change of dipoles. It can be interpreted as follows. As stated in section 2.2, when a sudden change occurs in the electric field, two effects follow: surface generation of electric charge which causes internal generation of a mechanical strain, and alignment of the domain orientation with the field. The first effect results in a rapid change of the PEA dimensions. The second effect does not remain when the external electric field is kept at the same level. The domain orientation changes back to the original direction slowly, which results in the surface charge increasing slowly. Thus, the displacement of the PEA experiences a slow drift after a sudden change. This can also explain why creep is reduced by utilizing charge control [26, 27]: the surface charge is maintained to be constant when the input charge from the
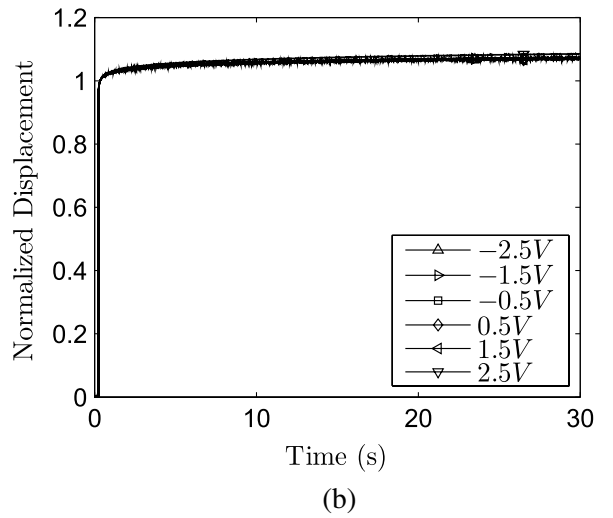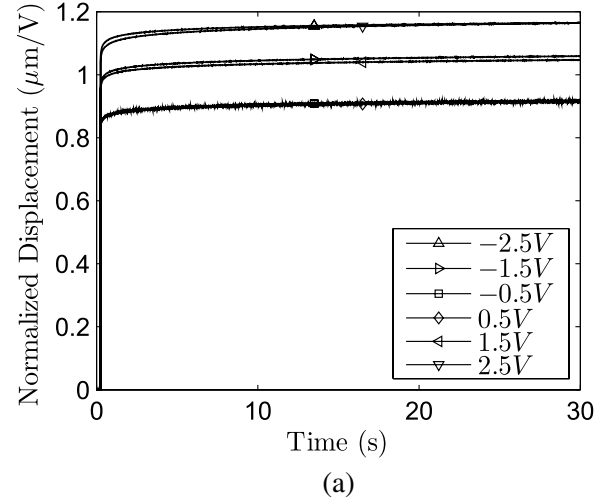

Figure 6. The observed creep and nonlinear gains behaviors in the case of step excitations: (a) responses normalized by input values, (b) responses normalized by both input values and nonlinear gains.

pump source stays at the same level, even if the domain orientation changes.

The slow change of the domain orientation is caused by the memory effect, which is appropriate to be modeled as a fractional-order system [28]. A fractional-order integrator (with the order between 0 and 1) causes a drift, which is ideal to describe the creep phenomenon. The smaller the order, the slower the creep motion will be. In fact, the dielectric materials are not ideal resistors or capacitances. They exhibit a fractional behavior yielding electric impedances of the form $1/[(jw)^\alpha C_F]$ with $\alpha \in \mathcal{R}^+$ [15, 29]. In [14] the PEA is modeled as resistocaptance [30]—an element whose property is between the resistor and the capacitance—to characterize its creep. Herein, the creep is described by a fractional-order system, with the constitutive equation described by [14, 28, 30]

$$_{t_0}\mathbf{D}_t^\alpha q(t) = Ku(t), \qquad 0 \leq \alpha \leq 1 \quad (18)$$

where the element is pure conductance with $K = G$ S for $\alpha = 1$, and pure capacitor with $K = C$ F for $\alpha = 0$. Provided

that a PEA is relaxed at $t = 0$, the relationship between the input charge q and the driving voltage u in the s-domain can be described by

$$\frac{Q(s)}{U(s)} = \frac{K}{s^\alpha}. \tag{19}$$

More details on this can be found in [28, 31, 32].

2.3.3. Integrated model for creep and hysteresis. Considering the slow drift of the domain orientations, the voltage-limited capacitors and ideal capacitor in figure 5 are replaced by resistocaptances. That is to say that the linear relationship between charge and voltage in equation (16) is replaced by the fractional-order dynamics in equation (18). Then, one obtains the FOMRC model as

$$\frac{\dot{q}_i(t)}{T_e} = \begin{cases} \dot{x}(t) & u_i(t)\mathrm{sgn}\,[\dot{q}(t)] < u_{S,i} \\ 0 & u_i(t)\mathrm{sgn}\,[\dot{q}(t)] \geq u_{S,i} \end{cases} \tag{20}$$

$$_{t_0}\mathbf{D}_t^{\alpha_i}\frac{q_i(t)}{T_e} = \kappa_i u_i(t), \qquad 0 \leq \alpha_i \leq 1 \tag{21}$$

$$u(t) = \sum_{i=1}^{n+1} u_i(t). \tag{22}$$

Based on the analysis in section 2.3.1, it is assumed that the fractional dynamics of all the elements are of the same order, i.e. $\alpha_1 = \alpha_2 = \cdots = \alpha_{n+1} = \alpha$. Noting that when a voltage-limited capacitor is unsaturated, its charge change rate equals that of the total network, i.e. $\dot{q}_i = \dot{q}$ if $|u_i| \leq u_{S,i}$, then one can obtain that

$$\dot{u}(t) = {}_{t_0}\mathbf{D}_t^\alpha \dot{q}(t) \sum_{i=m+1}^{n+1} \frac{1}{K_i} \tag{23}$$

where m is the number of saturated elements. For a sufficient small time duration Δt, equation (23) can be approximated by

$$\Delta u(t) = {}_{t_0}\mathbf{D}_t^\alpha \Delta q(t) \sum_{i=m+1}^{n+1} \frac{1}{K_i} \tag{24}$$

which further yields to

$$_{t_0}\mathbf{D}_t^\alpha \Delta q(t) = \frac{\Delta u(t)}{\sum_{i=m+1}^{n+1} \frac{1}{K_i}}. \tag{25}$$

The right-hand term implies that the change of voltage is distributed on these unsaturated elements inversely proportional to the gain K_i. Noting that the $(n+1)$th element is never saturated, the equation is further simplified as

$$_{t_0}\mathbf{D}_t^\alpha q(t) = K_{n+1}u_{n+1}. \tag{26}$$

This equation indicates that the hysteresis and creep in a PEA can be modeled separately. The FOMRC model now is simple and easy to be implemented: first calculating the applied voltage distribution based on the MRC model and then computing the charge on the last element based on fractional-order integrator.
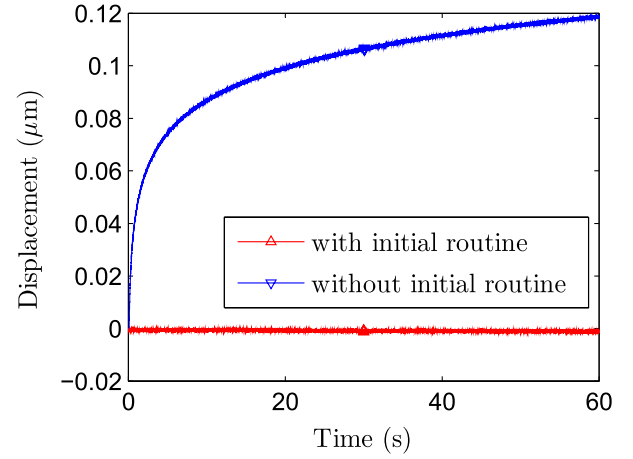

Figure 7. Displacement under zero input with and without initial routine.

3. Parameter identification and optimization

In this section, the routine for parameter identification is given, including the data collection, initial parameter calculation, and the parameter optimization.

3.1. Data collection

Before the data are collected, an initial routine is applied first to drive all the elements to zero position. The input of this initial routine is a stepwise amplitude-decreased signal, as given by

$$u(t) = a(t)\sin(\omega t - \pi/2) \tag{27}$$

$$a(t) = \begin{cases} u^{\max} - k_1 t & 0 \leq t \leq t_1 \\ a(t_1)\exp(k_2(t_1 - t)) & t_1 < t \leq t_f \end{cases} \tag{28}$$

where $u^{\max}$ is the maximum input applied on the PEA, t_f is the initial routine end time, and k_1, k_2, and t_1 are the designed parameters satisfying that $k_1, k_2 > 0$ and $k_1 = k_2(a^{\max} - k_1 t_1)$.

After this initial routine, the PEA is in the relaxed state. This initial routine solves the uncertainty of internal states of the MRC model and fills the initial relaxed state requirement of the fractional-order system. Figure 7 shows the PEA's zero input responses with and without the initial routine. Without applying the initial routine, the initial internal states are not zero, then the fractional-order dynamics causes a slow drift in the displacement. As the initial internal states are unknown and random, the drift is different for each run and unpredictable. However, with the initial routine, the drift reduces greatly. The effect of the initial routine can also be seen from the hysteresis loop, as shown in figure 8. Without the initial routine, the nonzero internal states cause that the initial increase curve (the red thick line) is not from the origin, whereas with the initial routine this curve initiates from the origin.

Then a triangular excitation and a staircase input with stepwise decreasing amplitude are applied to the PEA. The input and output data are collected at a sampling rate of 1 kHz and are shown in figure 9. The triangular signal has the slope
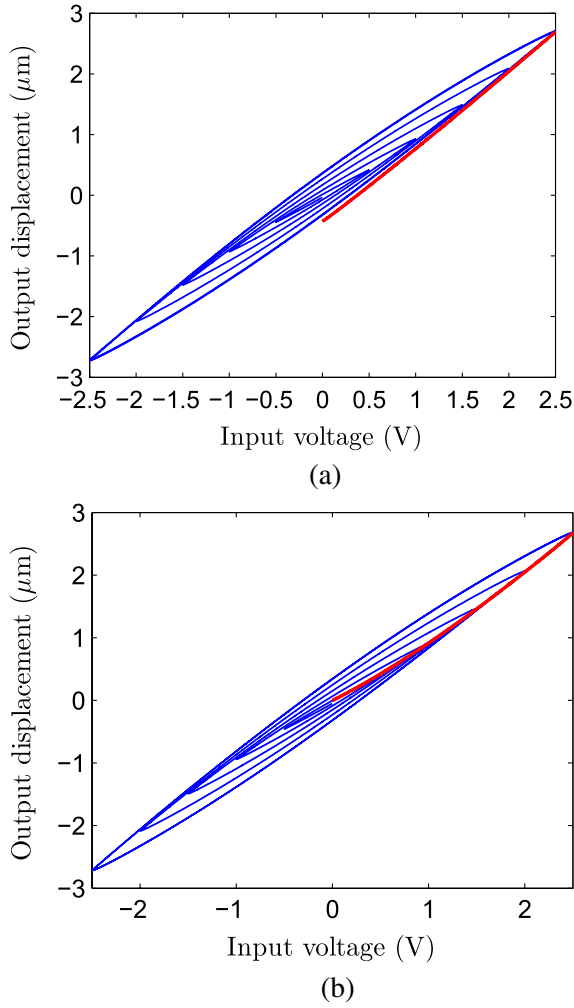
6

(a)

(b)

Figure 8. Hysteresis loop (a) with and (b) without initial routine.
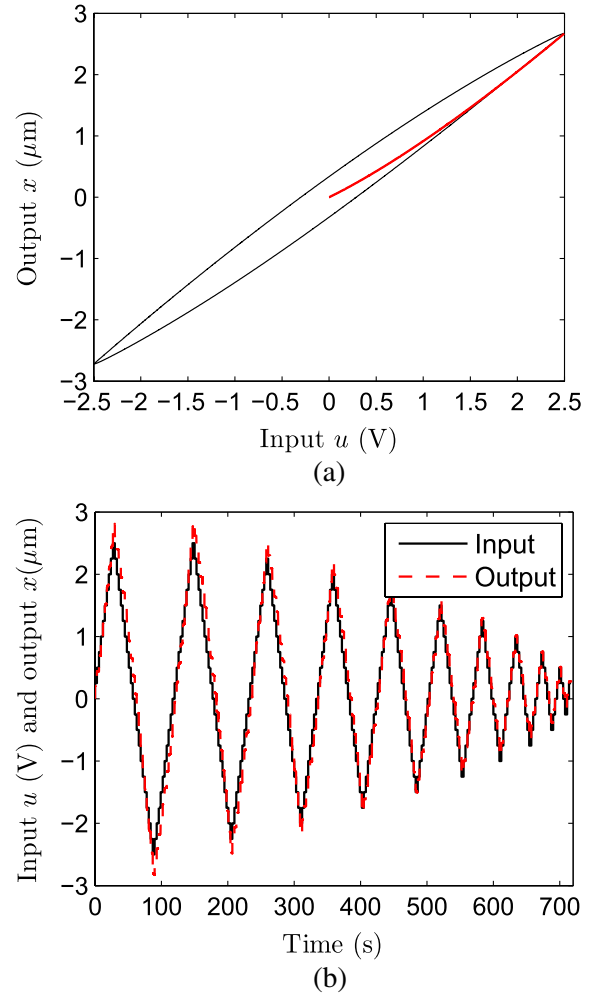

(a)

(b)

Figure 9. Collected data for parameter identification: (a) hysteresis loop in the case of triangular excitation, (b) displacement response in the case of staircase excitation.

of 1 V s^{-1}, at which speed the effects of mechanical resonance and creep can be ignored. The initial rising curve, the bold line in figure 9(a), generated by this signal is used to calculate the initial parameters of the MRC model. For the staircase input, each step is with an amplitude of 0.25 V and lasts for 3 s. The response of this type of signal couples effects of both hysteresis and creep. Thus it is used for parameter optimization of the FOMRC model.

3.2. Parameter calculation and optimization

The initial MRC parameters are calculated from a piecewise linear fit of the initial rising curve with $n + 1$ linear elements [12, 13, 22]. This can be done by fitting the initial rising curve, the bold line in figure 9(a), by a polynomial function, $u = p(x)$, with an appropriate degree. Divide the interval $[0, x^{\max}]$ into n equally spaced segments, with the length of each segment equaling to $\Delta x = x^{\max}/n$. Then one has

$$\sum_{i=j}^{n+1} \frac{1}{\kappa_i} \approx \frac{\mathrm{d}p}{\mathrm{d}x}\left[\left(j - \frac{1}{2}\right)\Delta x\right], \qquad j = 1, 2, \ldots, n. \quad (29)$$

If the transfer ratios and the effective capacitance of the PEA are provided, κ_{n+1} can be calculated and, then, κ_i, $i = 1, 2, \ldots, n$, are obtained. Unfortunately, these transfer ratios are seldom provided by the manufacturer and the effective capacitance provided is measured under small-signal values [25], which is different from that used in the MRC model. What is worse, is that it is difficult to measure these parameters for some commercially available PEAs. In this paper, κ_{n+1} is approximated from $\frac{\mathrm{d}p}{\mathrm{d}x}(x^{\max})$, i.e. $\frac{1}{\kappa_{n+1}} \approx \frac{\mathrm{d}p}{\mathrm{d}x}(x^{\max})$. The saturated voltages $u_{S,i}$ are calculated from

$$u_{S,i} = p(i \cdot \Delta u)/\kappa_i, \qquad i = 1, 2, \ldots, n. \quad (30)$$

As the $(n+1)$th element never saturates, $u_{S,n+1}$ is selected as a fixed sufficient large voltage.

In this application, the following five-order polynomial function is used to fit the initial rising curve.

$$\begin{aligned} u &= p(x) \\ &= 4.01 \times 10^{-6}x^5 - 2.24 \times 10^{-4}x^4 + 5.25 \times 10^{-3}x^3 \\ &\quad - 0.0764x^2 + 1.99x + 0.0102. \end{aligned} \quad (31)$$

Table 1. Identified FOMRC model parameters.

i	$u_{S,i}$ (V)	κ_i (μm V^{-1})
1	0.0368	10.4571
2	0.0364	23.6702
3	0.0370	19.4110
4	0.0168	7.6675
5	0.0432	37.6126
6	0.0320	41.2519
7	0.0525	36.6254
8	0.0262	49.9662
9	0.0167	64.0682
10	0.1036	24.7827
11	—	1.2808

Then, by setting $n = 10$, κ_i and $U_{S,i}$ are calculated from equations (29) and (30), respectively.

The initial fractional-order is identified using the double-logarithmic creep model [14] from step response. Based on the double-logarithmic creep model and with the unit step input, the output displacement satisfies

$$x(t)|_{t \geq t_c} = \frac{bt^\alpha}{\alpha \Gamma(\alpha)} \quad (32)$$

which can be rewritten as

$$\log x(t)|_{t \geq t_c} = \alpha \log t + \log \frac{b}{\alpha \Gamma(\alpha)} \quad (33)$$

where $t_c = 0.1$ s is the time from which the effect of the mechanical resonance can be ignored. Then the fractional-order α can be estimated with the least square method. Details can be found in [14].

These parameters are then optimized by solving the following minimization problem

$$\min_{\kappa_1, \ldots, \kappa_{n+1}, u_{S,1}, \ldots, u_{S,n}, \alpha} \sum_{k=1}^{N} [x(t_k) - \text{FOMRC}[u](t_k)]^2 \quad (34)$$

where N is the number of samples, and FOMRC refers to the FOMRC model operator. As stated previously, the response to the staircase like signal contains effects of hysteresis and creep. So the input voltage and output displacement of a staircase excitation, see figure 9(b), is served as the source data for optimization. A Simulink model is built to simulate the FOMRC model operator. Then the MATLAB function `fmincon` is used to search for the optimal parameters with the initial parameters calculated above. All the unknown parameters are involved. The identified fractional-order is 0.015 and other parameters are given in table 1.

4. Experimental results and discussion

4.1. Experimental setup

Experiments are conducted with the piezo nanopositioner PI-753.1CD Physik Instrumente. It is integrated with a capacitive sensor driven by an E-625 piezo controller. The data acquisition and control card is PCI-6289 from National Instruments Corporation, with 18-bit A/D channels and 16-bit
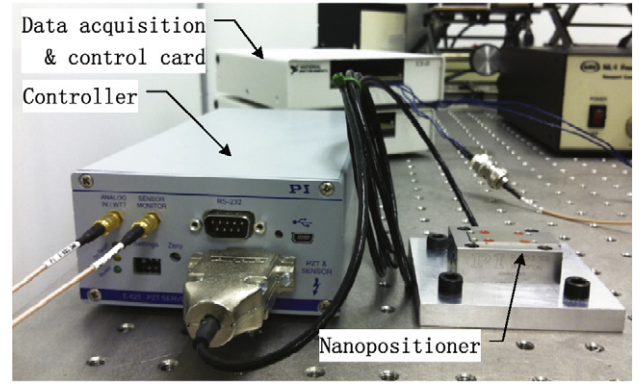
Figure 10. Experimental system.
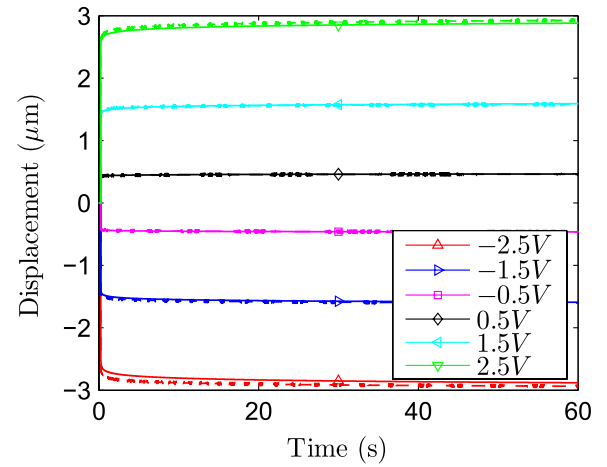
Figure 11. Measured (dashed line) and simulated (solid line) displacements in the case of step excitation with different amplitudes.

Table 2. Comparison of measurement and simulation for step excitation.

Input voltage (V)	2.5	1.5	0.5	−0.5	−1.5	−2.5
Displacement NRMSE (%)	1.50	0.44	0.69	0.43	1.07	2.28

D/A channels. Figure 10 shows the experimental system located at SDCNLab of York University. Experiments are carried out by using Simulink and xPC Target at room temperature. The program is compiled on the host computer, and then downloaded to the target computer and runs in real-time environment.

4.2. Model validation

Firstly, a set of step signals with different amplitudes are applied. The simulated and measured results are shown in figure 11. The normalized root mean square error value (NRMSE), calculated as a ratio of the root mean square error to the measured displacement at 60 s, is given in table 2. The NRMSE errors range from 0.43% to 2.28%, which is slightly more accurate than the high-order model proposed in [33].
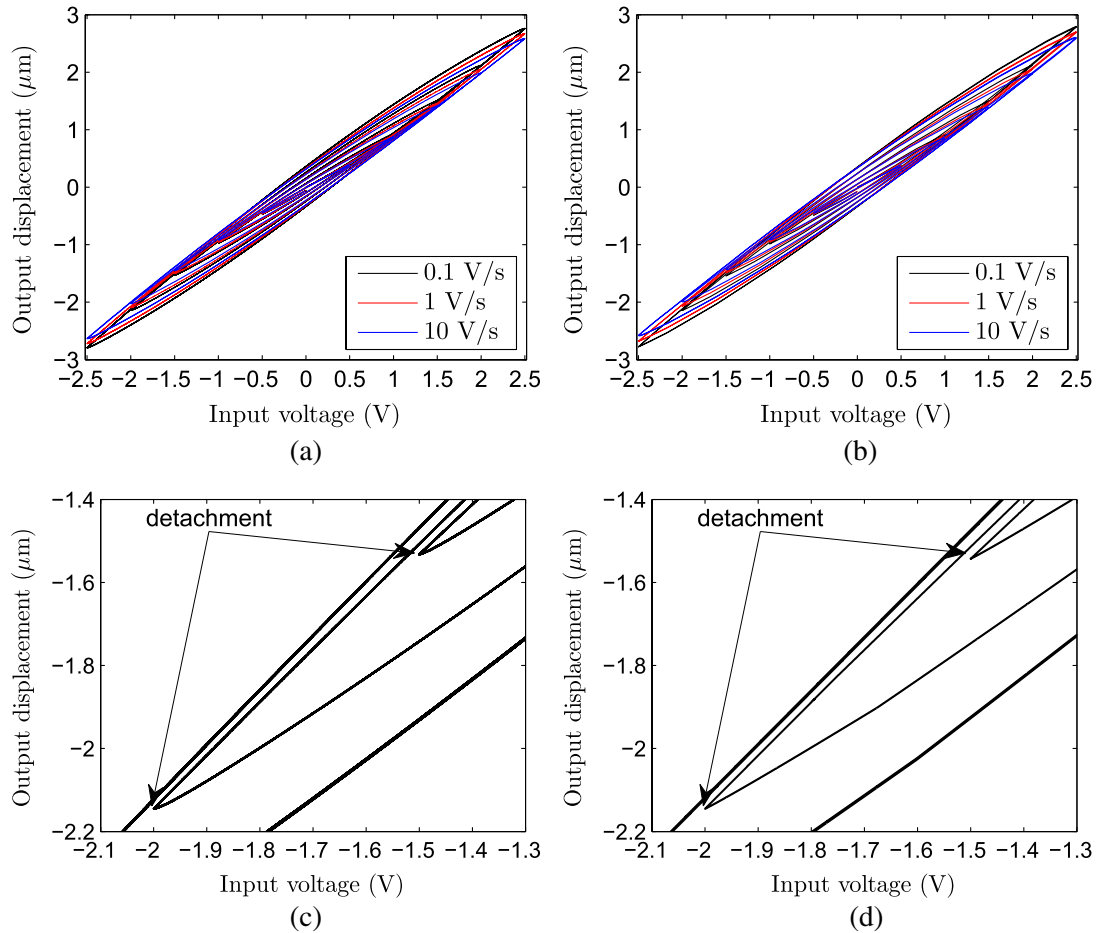
Figure 12. Experimental and simulated rate-dependent hysteresis behavior and detachment of loops: (a) experimental hysteresis loops, (b) measured hysteresis loops, (c) experimental loops' detachment, (d) measured loops' detachment.

In [23], Yeh *et al* provided the result with the error less than 0.3% in the case of a 200 V step response. However, the model is very complicated with 38 parameters. Meanwhile, results with different input amplitudes cannot be found in that paper. Thus, the FOMRC model can characterize effects of both nonlinear gain and creep.

The hysteresis is usually modeled as rate-independent. However, the observed hysteresis behaviors in PEAs have a rate-dependent feature. To show this, the PEA is excited by triangular excitations with decreasing amplitude and different slopes. From the experimental results in figure 12(a), one can notice that as the slopes of the input signal increase, the hysteresis loop not only gets shorter and wider, but also tends to rotate clockwise as a whole. Meanwhile, from the zoom-in plot in figure 12(c), one can also notice that the minor hysteresis loop detaches from the major one. Both phenomena are caused by the coupling effects of hysteresis and creep. They cannot be described by only quasi-static elements, such as play operator [5–11] or MRC element [12, 13, 21]. By introducing the fractional-order integrator dynamics, the FOMRC model can describe both phenomena, as shown in figures 12(b) and (d). The error histories with respect to normalized time (by the real time divided by the period of the first circle of the triangular signal) are shown in figure 13. More results for similar signals but with different voltage
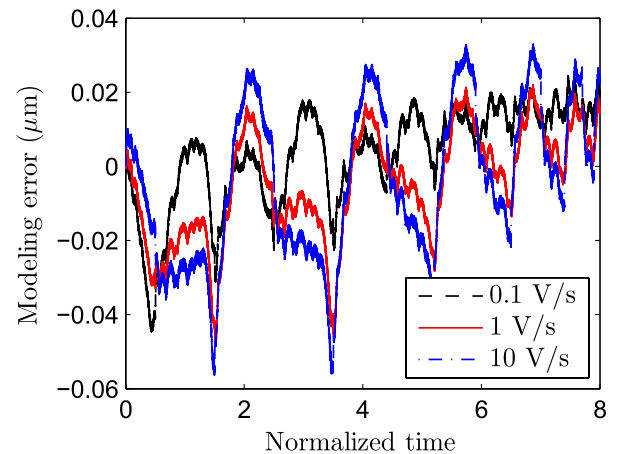

Figure 13. Model error histories in the case of triangular excitations with decreasing amplitude and different slopes.

change rates are given in table 3. The NRMSE of the model is very small, even for rapid changes of displacement by noting that the displacement change rate approximates 1.2 μm s^{-1} if the rate of input is 1.0 V s^{-1}. These results show that the FOMRC model is robust to the voltage change rate.

9

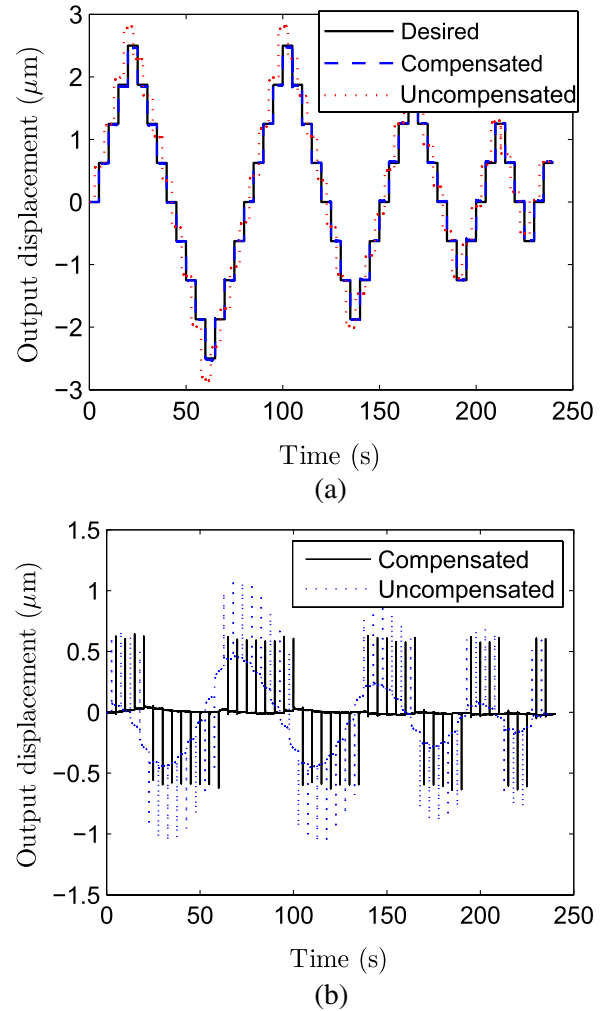**Table 3.** Comparison of measurement and simulation for triangular excitation.

Voltage slope (V s^{-1})	0.1	0.5	1	2	5	10	20	50	100	200
Displacement NRMSE (%)	0.25	0.25	0.29	0.32	0.33	0.40	0.54	0.95	1.64	3.03
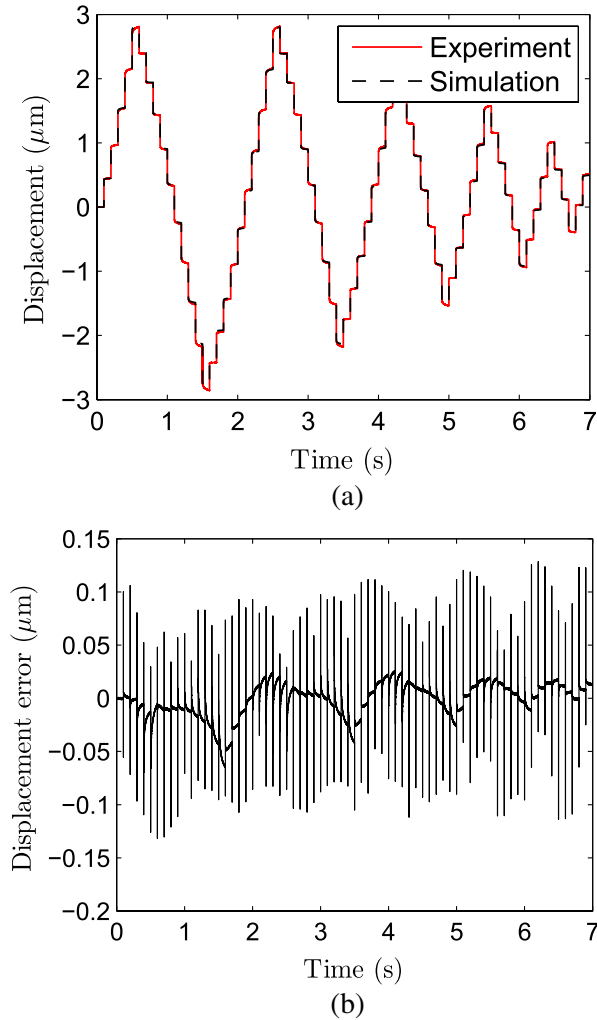
Figure 14. Displacement responses and error history in the case of staircase excitation: (a) displacement response, (b) error history.

Figure 15. Tracking control with and without hysteresis and creep compensation under open-loop operation: (a) displacement response, (b) error history.

For the staircase input, both creep and hysteresis effects exist. The comparison between experimental and simulated results is shown in figure 14. The model is still able to closely match the actual PEA's output response. According to the error response shown in figure 14(b), except for the transience occurring shortly at the beginning of each step, the maximum error is about 0.05 μm, with NRMSE as 0.29%.

4.3. Compensation for hysteresis and creep

Equations (20)–(22) describe a general relationship between the input voltage and the output displacement. Based on this, not only the FOMRC model, but also the inverse FOMRC model can be constructed. Actually, the inverse FOMRC model is much easier to build than the FOMRC model. As

stated in section 2.3.3, for FOMRC model construction, an iteration is required to calculate the distribution of the applied voltage on each element based on the MRC model given in equations (15)–(17). If the desired displacement is served as input, the output voltage of each element is calculated directly based on equations (20) and (21) and, then, the total output voltage is given by equation (22). In other words, the inverse FOMRC model is constructed directly, without any iterations.

The hysteresis and creep are compensated for by using the inverse FOMRC model. Figure 15 shows the results with different strategies. It can be seen that the compensated PEA follows the desired position closely. The NRMSE is reduced from 5.04% in the uncompensated case to 0.36% in the compensated case.
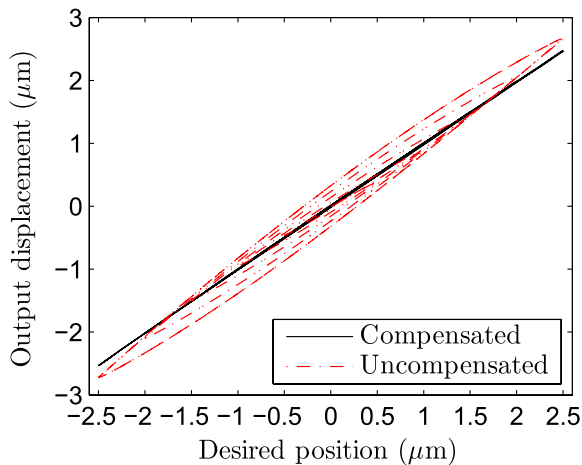
Figure 16. Linearization of PEA characteristics with inverse model.

The input–output character of the compensated PEA with excitation of a triangular signal of decreasing amplitude is shown in figure 16. An excellent linear result can be observed in figure 16. The nonlinear error amounts to only 0.65%, reduced from 12.06% in the uncompensated case.

4.4. Discussion

The MRC model and the fractional-order dynamics can capture the rate-independent hysteresis and creep, respectively. By integrating them, the FOMRC model is able to simultaneously capture both phenomena and their coupling effects, i.e. rate-dependent hysteresis phenomenon and detachment of hysteresis loops. This has been verified through experiments. However, as the high-frequency dynamics, such as the mechanical resonance and the amplifier behavior, is ignored, the FOMRC model can hardly capture the dynamics at high frequencies. Fortunately, high-frequency dynamics can be modeled separately using a linear system, which is outside the scope of this paper. As the inverse FOMRC model can be constructed directly, it is quite suitable for compensation for creep and hysteresis in the open-loop application. As the creep is a long-term effect, it can be well compensated by feedback techniques. Thus, for the closed-loop application, the FOMRC model has little or no advantage over the MRC model. Actually, compared to the MRC model, the FOMRC model results in a higher computational burden.

5. Conclusion

In this paper, a fractional-order Maxwell resistive capacitor model is proposed to simultaneously characterize the creep and hysteresis. This model is obtained by integrating the fractional-order creep into the Maxwell resistive capacitor model. The physical interpretation of the Maxwell resistive capacitor model in the electric domain is given in detail, based on which the physical model for the PEA is modified and the associated identification procedure is developed. The proposed model is examined by sufficient experimental tests and the experimental results show that it is able to

characterize the rate-dependent hysteresis, the detachment of hysteresis loops, and the creep. This model is robust to the rate change of the input. Moreover, an inverse model is built based on the fractional-order Maxwell resistive capacitor model for the open-loop control application. With this inverse model compensation, experiments show that the nonlinear displacement error has been reduced to 0.65%, compared to 12.06% in the uncompensated case.

References

[1] Minase J, Lu T F, Cazzolato B and Grainger S 2010 A review, supported by experimental results, of voltage, charge and capacitor insertion method for driving piezoelectric actuators *Precis. Eng.* **34** 692–700
[2] Jang M-J, Chen C-L and Lee J-R 2009 Modeling and control of a piezoelectric actuator driven system with asymmetric hysteresis *J. Franklin Inst.* **346** 17–32
[3] Liu L, Tan K K, Chen S, Teo C S and Lee T H 2013 Discrete composite control of piezoelectric actuators for high-speed and precision scanning *IEEE Trans. Indust. Inform.* **9** 859–68
[4] Croft D, Shedd G and Devasia S 2000 Creep, hysteresis, and vibration compensation for piezoactuators: atomic force microscopy application *Proc. American Control Conf. (June)* vol 3, pp 2123–8
[5] Kuhnen K 2005 Modelling, identification, and compensation of complex hysteretic and log (*t*)-type creep nonlinearities *Control Intell. Syst.* **33** 134–47
[6] Krejci P and Kuhnen K 2001 Inverse control of systems with hysteresis and creep *IEE Proc.* D **148** 185–92
[7] Kuhnen K and Janocha H 2000 Operator-based compensation of hysteresis, creep and force-dependence of piezoelectric stack actuators *Proc. 1st IFAC Conf. on Mechatronic Systems (Sept.)* pp 421–6
[8] Janocha H and Kuhnen K 2000 Real-time compensation of hysteresis and creep in piezoelectric actuators *Sensors Actuators* A **79** 83–9
[9] Pesotski D, Janocha H and Kuhnen K 2010 Adaptive compensation of hysteretic and creep non-linearities in solid-state actuators *J. Intell. Mater. Syst. Struct.* **21** 1437–46
[10] Mokaberi B and Requicha A A G 2008 Compensation of scanner creep and hysteresis for AFM nanomanipulation *IEEE Trans. Autom. Sci. Eng.* **5** 197–206
[11] Yang Q and Jagannathan S 2009 Creep and hysteresis compensation for nanomanipulation using atomic force microscope *Asian J. Control* **11** 182–7
[12] Goldfarb M and Celanovic N 1997 Modeling piezoelectric stack actuators for control of micromanipulation *IEEE Control Syst.* **17** 69–79
[13] Goldfarb M and Celanovic N 1997 A lumped parameter electromechanical model for describing the nonlinear behavior of piezoelectric actuators *J. Dyn. Syst. Meas. Control* **119** 479
[14] Liu Y, Shan J and Qi N 2013 Creep modeling and identification for piezoelectric actuators based on fractional-order system *Mechatronics* at press
[15] Westerlund S 1991 Dead matter has memory! *Phys. Scr.* **43** 174–9

[16] Aguirre G, Janssens T, Van Brussel H and Al-Bender F 2012 Asymmetric-hysteresis compensation in piezoelectric actuators *Mech. Syst. Signal Process.* **30** 218–31

[17] Al-Bender F, Lampaert V and Swevers J 2004 Modeling of dry sliding friction dynamics: from heuristic models to physically motivated models and back *Chaos* **14** 446–60

[18] Rizos D D and Fassois S D 2004 Presliding friction identification based upon the Maxwell slip model structure *Chaos* **14** 431–45

[19] Rizos D D and Fassois S D 2009 Friction identification based upon the LuGre and Maxwell slip models *IEEE Trans. Control Syst. Technol.* **17** 153–60

[20] Al-Bender F, Lampaert V and Swevers J 2005 The generalized Maxwell-slip model: a novel model for friction simulation and compensation *IEEE Trans. Autom. Control* **50** 1883–7

[21] Yeh T-J, Lu S-W and Wu T-Y 2006 Modeling and identification of hysteresis in piezoelectric actuators *J. Dyn. Syst. Meas. Control* **128** 189–96

[22] Juhász L, Maas J and Borovac B 2011 Parameter identification and hysteresis compensation of embedded piezoelectric stack actuators *Mechatronics* **21** 329–38

[23] Yeh T-J, Hung R-F and Lu S-W 2008 An integrated physical model that characterizes creep and hysteresis in piezoelectric actuators *Simul. Modelling Pract. Theory* **16** 93–110

[24] Georgiou H and Mrad R B 2006 Electromechanical modeling of piezoceramic actuators for dynamic loading applications *J. Dyn. Syst. Meas. Control* **128** 558–67

[25] Physik Instrumente (PI) GmbH & Co. 2009 *Piezoelectrics In Positioning* www.physikinstrumente.com/en/pdf_extra/2009_PI_Piezo_University_Designing_with_Piezo_Actuators_Tutorial.pdf

[26] Ma Y T, Huang L, Liu Y B and Feng Z H 2011 Note: creep character of piezoelectric actuator under switched capacitor charge pump control *Rev. Sci. Instrum.* **82** 046106

[27] Minase J, Lu T-F, Cazzolato B and Grainger S 2010 A review, supported by experimental results, of voltage, charge and capacitor insertion method for driving piezoelectric actuators *Precis. Eng.* **34** 692–700

[28] Das S 2011 *Functional Fractional Calculus* 2nd edn (Berlin: Springer) pp 1–99 231–4, 322–86

[29] Westerlund S and Ekstam L 1994 Capacitor theory *IEEE Trans. Dielectr. Electr. Insul.* **1** 826–39

[30] Bohannan G W, Hurst S K and Spangler L 2006 Electrical component with fractional order impedance *US Patent Specification* 20060267595, March 10

[31] Chen Y Q, Petras I and Xue D 2009 Fractional order control—a tutorial *Proc. American Control Conf. (June)* pp 1397–411

[32] Monje C A, Chen Y, Vinagre B M, Xue D and Feliu-Batlle V 2010 *Fractional-Order Systems and Controls: Fundamentals and Applications* (*Springer Advances in Industrial Control*) (Berlin: Springer)

[33] Richter H, Misawa E A, Lucca D A and Lu H 2001 Modeling nonlinear behavior in a piezoelectric actuator *Precis. Eng.* **25** 128–37